

A compendium of AGN inclinations with corresponding UV/optical continuum polarization measurements

F. Marin^{*}

Astronomical Institute of the Academy of Sciences, Boční II 1401, CZ-14100 Prague, Czech Republic

Accepted 2014 March 21. Received 2014 March 21; in original form 2013 December 12

ABSTRACT

The anisotropic nature of active galactic nuclei (AGN) is thought to be responsible for the observational differences between type-1 (pole-on) and type-2 (edge-on) nearby Seyfert-like galaxies. In this picture, the detection of emission and/or absorption features is directly correlated to the inclination of the system. The AGN structure can be further probed by using the geometry-sensitive technique of polarimetry, yet the pairing between observed polarization and Seyfert type remains poorly examined. Based on archival data, I report here the first compilation of 53 estimated AGN inclinations matched with ultraviolet/optical continuum polarization measurements. Corrections, based on the polarization of broad emission lines, are applied to the sample of Seyfert-2 AGN to remove dilution by starburst light and derive information about the scattered continuum alone. The resulting compendium agrees with past empirical results, i.e. type-1 AGN show low polarization degrees ($P \leq 1\%$) predominantly associated with a polarization position angle parallel to the projected radio axis of the system, while type-2 objects show stronger polarization percentages ($P > 7\%$) with perpendicular polarization angles. The transition between type-1 and type-2 inclination occurs between 45° and 60° without noticeable impact on P . The compendium is further used as a test to investigate the relevance of four AGN models. While an AGN model with fragmented regions matches observations better than uniform models, a structure with a failed dusty wind along the equator and disc-born, ionized, polar outflows is by far closer to observations. However, although the models correctly reproduce the observed dichotomy between parallel and perpendicular polarization, as well as correct polarization percentages at type-2 inclinations, further work is needed to account for some highly polarized type-1 AGN

Key words: polarization – radiative transfer – scattering – atlases – galaxies: active – galaxies: structure.

1 INTRODUCTION

The unified model of active galactic nuclei (AGN; Antonucci 1993) states that most of the observational differences between type-1 and type-2 Seyfert-like galaxies arise from an orientation effect. According to this theory, the disappearance of ultraviolet (UV) and optical broad emission features at type-2 inclinations can be explained by the presence of an obscuring, circumnuclear material along the equatorial plane of the AGN (the so-called dusty torus) that hides both the central engine and the photoionized broad line regions (BLRs; the low ionization line LIL BLR and the highly ionized line HIL BLR; Rowan-Robinson 1977; Osterbrock 1978). A type-2 viewing angle can then be defined as a line of sight towards the central source that intercepts

the equatorial dust, while type-1 inclination allows a direct view of the central engine. The observational lack of type-1 AGN with edge-on host galaxy (Keel 1980; Lawrence & Elvis 1982) suggests that dust along Seyfert 1 galaxy discs may obscure the HIL and LIL BLR and make the AGN appear like Seyfert 2s (Maiolino & Rieke 1995). The number count of Seyfert 1 objects is thus expected to be small, even if the fraction of type-1 against type-2 AGN in the nearby Universe still needs to be properly determined. Estimating the orientation of a large sample of AGN is necessary to verify the assumptions of the unified model, and check whether all the differences between Seyfert 1 and Seyfert 2 objects can be explained by inclination or if morphological differences must also be taken into account.

In this regard, polarization has proven to be a solid tool to investigate the inner structure of AGN. The spectropolarimetric measurements of NGC 1068 by Miller &

^{*} frederic.marin@asu.cas.cz

Antonucci (1983) helped to identify electron and dust scattering as the main mechanisms producing a continuum polarization in radio-quiet AGN. Going further, the extensive high-resolution, high signal-to-noise spectropolarimetric observation of the same AGN by Antonucci & Miller (1985) revealed the presence of highly polarized, broad, symmetric Balmer and permitted Fe II lines. The polarization spectrum was found to be closely similar to typical Seyfert 1 galaxies, supporting the idea that Seyfert 2 AGN are hiding Seyfert 1 core behind the dusty torus. This discovery was a key argument in favour of a unified model of AGN.

Spectropolarimetry is thus a powerful method to probe the validity of any AGN model, as the computed fluxes shall match both observational intensity, polarization percentage and polarization angle, reducing the number of free parameters/degeneracies (Kartje 1995; Young 2000; Goosmann & Gaskell 2007; Marin et al. 2012a). In order to model a peculiar source, the observer’s viewing angle i has to be set (e.g. $i \sim 70^\circ$ for NGC 1068; Hönig et al. 2007; Raban et al. 2009) to explore the resulting polarization (Goosmann & Matt 2011; Marin, Goosmann & Dovčiak 2012). The impact of the system’s orientation on to the net polarization can lead to significantly different results, especially when the observer’s line of sight matches the half-opening angle of the obscuring region (Marin et al. 2012a). To be consistent with observation, an investigation of the model over a broad range of inclination must be undertaken. However, any comparison between the observed polarization and the theoretical orientation of individual AGN is hampered by the lack of a data base that combines inclination and polarization.

It is the aim of this paper to provide the first spectropolarimetric compendium of Seyfert-like galaxies, gathering observed continuum polarizations from literature correlated with estimated inclinations of individual AGN. In Sect. 2, I investigate the different observational and numerical techniques used to estimate the inclination of 53 objects, and match the sources with their archival UV/optical polarization measurement, whenever it is feasible. To illustrate the significance of this catalogue when comparing models to observations, in Sect. 3, I pick four different, competitive AGN models from the literature and analyse them in the framework of this compendium. In Sect. 4, I review the successes and potential improvements of AGN modelling, explore the problematic, high polarization levels of peculiar type-1 objects and discuss possible bias on the estimation of inclination. Finally, conclusions are drawn in Sect. 5.

2 THE COMPENDIUM

While polarimetric measurement of AGN are difficult to obtain due to intrinsically low polarization degrees in type-1 objects (Berriman 1989; Berriman et al. 1990; Smith et al. 2002a) and flux dilution by unpolarized starlight in type-2s (Antonucci 2002a), it is more straightforward to measure polarization than to estimate the inclination of the system, as orientation is not easily derived directly from observations. Hence, the following sections present different techniques to infer the orientation of AGN (with potential caveats discussed in Sect. 4.3), the selection criteria used to select/remove estimated inclinations, corrections that have to be made to most of the Seyfert-2 AGN and the final com-

pilation of data. For the remaining of this paper, the terminology “inclination of the system” will refer to the nuclear, not the host, inclination.

2.1 Estimation of the system’s inclination

METHOD A. Based on the tight correlation found by Gebhardt et al. (2000), Ferrarese & Merritt (2000) and Merritt & Ferrarese (2001) between the mass of the central supermassive black hole and the bulge velocity dispersion in nearby galaxies, Wu & Han (2001) and Zhang & Wu (2002) developed a method to derive the inclination angle of nearby Seyfert 1 AGN. By assuming a Keplerian motion of the LIL BLR and a similar mass/velocity dispersion between type-1 AGN and regular galaxies, they estimated the orientation angles i for a variety of Seyfert 1 objects, with associated errors calculated from the uncertainties of both the black hole mass (obtained by reverberation mapping techniques; Blandford & McKee 1982) and the measured velocity dispersion.

METHOD B. The inclination estimation of the Seyfert 1 galaxy ESO 323-G077 comes from the optical spectropolarimetric measurement achieved by Schmid, Appenzeller & Burch (2003), who detected very high levels of linear polarization (up to 7.5 % at 3600 Å). Within the framework of the unified model, those levels are inconsistent with the polarization degrees produced by an object seen in the polar orientation (Marin et al. 2012a). Schmid, Appenzeller & Burch (2003) argued that the system must be partially hidden by the dusty torus and tilted by $\sim 45^\circ$ with respect to the observer’s line of sight to produce such a high polarization degree. The same method was previously applied to Fairall 51 (continuum polarization 4.12 % \pm 0.03 %) by Schmid et al. (2001), who also derived an inclination of $\sim 45^\circ$.

METHOD C. An increasing amount of X-ray bright, type-1 AGN shows an asymmetrically blurred emission feature at 6.4 keV, associated with iron fluorescence in near-neutral material (Reeves et al. 2006). Interestingly, the line broadening caused by Doppler effects and gravitational plus transverse redshifts can be used to numerically probe the inclination of the system (Fabian et al. 1989). In Nandra et al. (1997), this characteristic line profile is equally fitted within a Schwarzschild or a Kerr metric (even if recent modelling seems to favour maximally rotating black holes in the centre of type-1 AGN; Bambi 2011, 2013), giving a mean Seyfert 1 inclination of 30° .

METHOD D. Constraints on the inclination of NGC 1097 are derived by Storchi-Bergmann et al. (1997), who applied an eccentric accretion ring model to the observed broad, double-peaked Balmer emission lines. Between 1991 and 1996, the double-peaked H α line of NGC 1097 evolved from a red-peak dominance (Storchi-Bergmann et al. 1993) to a nearly symmetrical profile (Storchi-Bergmann et al. 1995) and up to a blue-peak dominance (Storchi-Bergmann et al. 1997). This line profile evolution can be explained by a refinement of the precessing, planar, elliptical accretion-ring model developed by Storchi-Bergmann et al. (1995) and Eracleous et al. (1995), to fit the data using an eccentric accretion disc inclined by 34° .

METHOD E. Hicks & Malkan (2008) measured the two-dimensional distribution and kinematics of the molecular, ionized, and highly ionized gas in the inner regions of a

sample of radio-quiet, type-1 AGN using high spatial resolution, near-infrared (IR) spectroscopy. Based on a model developed by Macchetto et al. (1997), they assumed that a gravitational well, created by the combined action of a central supermassive black hole and a distant stellar population, is driving the circular motion of a coplanar thin disc, reproducing the observed emission line gas kinematics. Exploring four free parameters (disc inclination, position angle of its major axis, black hole mass and mass-to-light ratio), Hicks & Malkan (2008) statistically estimated the inclination of NGC 3227, NGC 4151 and NGC 7469 using a Bootstrap Gaussian fit (Efron 1979).

METHOD F. To determine the inclination of a sample of nearby AGN, Fischer et al. (2013) explored the three-dimensional geometry and kinematics of the narrow-line regions (NLRs) of AGN, observing both type-1 and type-2 objects. Resolved by [O III] imaging and long-slit spectroscopy, most of the AGN show a bi-conical structure which can be morphologically and kinematically constrained. However, to extract information about the AGN orientation, a kinematic model must be generated. Using uniform, hollow, bi-conical models with sharp edges, Fischer et al. (2013) were able to statistically derive a set of morphological parameters (including orientation) for 17 objects out of 53.

METHOD G. Relatively bright and situated in the nearby Universe, NGC 1068 is an archetypal Seyfert 2 galaxy, observed during the last fifty years. Taking advantage of past near and mid-IR photometric and interferometric observations (Jaffe et al. 2004; Wittkowski et al. 2004), Höning et al. (2007) applied a three-dimensional radiative transfer code to a clumpy, dusty structure in order to reproduce the observed spectral energy distribution (SED). Among new constraints on the bolometric luminosity and the IR optical depth of the torus, Höning et al. (2007) estimated the overall inclination of NGC 1068 to be close to 70° .

METHOD H. Borguet & Hutsemékers (2010) examined the generation of C IV line profiles in broad absorption line (BAL) quasars using a two-component wind model. By modelling a structure based on stellar wind laws and composed of axisymmetric, polar and equatorial outflows filled with 2-level atoms, they succeeded to reproduce a large set of BAL profiles and concluded that the viewing angle to the wind is generally large. Unfortunately, degeneracies in line profile fitting do not allow stronger constraints.

METHOD I. Finally, Wills et al. (1992) investigated their own polarimetric and photometric observations of the type-2 quasar IRAS 13349+2438 in the context of an axisymmetric distribution of scatterers to explain the alignment of polarization with the major axis of the host galaxy. Using a model of a dusty disc parallel to the plane of the galaxy, similar to a usual dusty torus, surrounding the continuum source and the LIL BLR, they showed that both the observed polarization in the continuum and in the broad H α line could be reproduced if the inclination of the observer is about 52° with respect to the symmetry axis of their model.

2.2 Selection criteria

Once inclinations are obtained, I match them with UV/optical spectropolarimetric measurements, whenever it was possible. The methods presented in Sect. 2.1 derive about 100 AGN orientations but only 53 of them have pub-

lished continuum polarization measurements. Moreover, not all of the estimated inclinations are unique and a selection has to be done whenever two methods, or more, give different estimations for the same AGN. Tab. 1 lists discrepancies of duplicate inclinations. Reasons for the choice of a given inclination are discussed below.

3C 120. The inclination of 3C 120 found by Nandra et al. (1997), $i = 88^{+2}_{-1}$, is rejected in favour of the estimation by Wu & Han (2001), who found $i = 21^{+9.3}_{-7.7}$, a result in a better agreement with the type-1 classification of 3C 120¹.

FAIRALL 9. Due to the huge error bars derived by Nandra et al. (1997) on the orientation of Fairall 9 (89^{+1}_{-49}), covering the full permitted range of inclination for a type-2 object plus a fraction of the permitted range of type 1s, the viewing angle computed by Zhang & Wu (2002) is favored.

IC 4329A. The inclination derived by Zhang & Wu (2002) in the case of IC 4329A (5.0°) is compatible within the error bars of the estimation computed by Nandra et al. (1997). The latest ($10^{+13.0}_{-10.0}$) is thus selected in order to concur with the two values.

MRK 279. Estimated inclinations of Mrk 279 are rather different between Zhang & Wu (2002), $i = 13.0^\circ$, and Fischer et al. (2013), $i = 35.0^\circ$, especially since they do not have overlapping error bars. The inclination derived by Fischer et al. (2013) is favoured as Zhang & Wu (2002) were not able to recover the measured stellar velocity dispersion of Mrk 279 and had to estimate it from the [O III] emission line, introducing another potential bias in their final AGN orientation.

MRK 509. The inclination estimated by Nandra et al. (1997) covers the whole range of inclination possible for an AGN (89^{+1}_{-89}) and therefore does not make much sense. The inclination of Mrk 509 by Zhang & Wu (2002) is thus selected.

NGC 3227. There are four different estimations for the viewing angle of NGC 3227. Two have very large error bars (Nandra et al. 1997; Wu & Han 2001) overlapping the two others estimates by Hicks & Malkan (2008) and Fischer et al. (2013). Since the two later inclinations are very similar but from totally different estimation methods, they are likely to be representative of the real inclination of NGC 3227. Hence I favour the one of Hicks & Malkan (2008), $14.2^\circ \pm 2.5^\circ$, which agrees with the value found by Fischer et al. (2013), 15.0° .

NGC 3516. The values estimated by Nandra et al. (1997), $i = 26^{+3}_{-4}$, and Wu & Han (2001), $i = 38.3^\circ \pm 7.6^\circ$, are not overlapping but still very close to each other. However, provided that Wu & Han (2001) had to artificially estimate the errors on the black hole mass for NGC 3516 while Nandra et al. (1997) derived it from their simulation, the estimation made by Nandra et al. (1997) is used.

NGC 3783. Similarly to the case of Mrk 279, estimations of the orientation of NGC 3783 are rather different between Zhang & Wu (2002) and Fischer et al. (2013) and, for the

¹ 3C 120 is a type-1, broad-line, X-ray bright radio galaxy showing an episodic superluminal jet outflow (Marscher et al. 2002). 3C 120 is sometimes included in radio-quiet AGN surveys as its X-ray spectrum shows a strong relativistic iron K α emission (Nandra et al. 1997).

Object	Type	i_{sel} ($^{\circ}$)	i_{rej} ($^{\circ}$)
3C 120	1	$22.0^{+9.3}_{-7.7}$ (Wu & Han 2001)	88^{+2}_{-1} (Nandra et al. 1997)
Fairall 9	1	35.0 (Zhang & Wu 2002)	89^{+1}_{-49} (Nandra et al. 1997)
IC 4329A	1	$10^{+13.0}_{-10.0}$ (Nandra et al. 1997)	5.0 (Zhang & Wu 2002)
Mrk 279	1	35.0 (Fischer et al. 2013)	13.0 (Zhang & Wu 2002)
Mrk 509	1	19.0 (Zhang & Wu 2002)	89^{+1}_{-89} (Nandra et al. 1997)
NGC 3227	1	14.2 ± 2.5 (Hicks & Malkan 2008)	15.0 (Fischer et al. 2013)
			21^{+7}_{-21} (Nandra et al. 1997)
			$37.5^{+17.3}_{-25.4}$ (Wu & Han 2001)
NGC 3516	1	26^{+3}_{-4} (Nandra et al. 1997)	38.3 ± 7.6 (Wu & Han 2001)
NGC 3783	1	15.0 (Fischer et al. 2013)	40^{+12}_{-40} (Nandra et al. 1997)
			38.0 (Zhang & Wu 2002)
NGC 4051	1	$19.6^{+10.4}_{-6.6}$ (Wu & Han 2001)	25^{+12}_{-4} (Nandra et al. 1997)
			10.0 (Fischer et al. 2013)
NGC 4151	1	9^{+18}_{-9} (Nandra et al. 1997)	19.8 ± 2.9 (Hicks & Malkan 2008)
			45 (Fischer et al. 2013)
			$60^{+30}_{-30.6}$ (Wu & Han 2001)
NGC 5548	1	$47.3^{+7.6}_{-6.9}$ (Wu & Han 2001)	10^{+80}_{-10} (Nandra et al. 1997)
NGC 7469	1	15.0 ± 1.8 (Hicks & Malkan 2008)	20^{+70}_{-20} (Nandra et al. 1997)
			13.0 (Zhang & Wu 2002)
NGC 1068	2	70.0 (Hönig et al. 2007)	85.0 (Fischer et al. 2013)

Table 1. Selected (i_{sel}) and rejected (i_{rej}) nuclear inclinations according to the selection criteria presented in Sect. 2.1.

same reasons, the value derived by Fischer et al. (2013) is selected. The inclination recovered by Nandra et al. (1997) for NGC 3783, covering the whole possible inclination range for type-1 objects, is discarded.

NGC 4051. Both estimations made by Nandra et al. (1997), $i = 25^{+12}_{-4}$, and Wu & Han (2001), $i = 19.6^{+10.4}_{-6.6}$, are compatible and their error bars nearly fully overlap. The viewing angle taken from Wu & Han (2001) having slightly higher error bars, this value is chosen to fully concur with the estimations from Nandra et al. (1997) and to be representative of the value derived by Fischer et al. (2013), 10.0° .

NGC 4151. The inclination angle of NGC 4151 derived by Wu & Han (2001) is not considered due to its huge error bars that cover two thirds of the possible AGN inclinations ($60^{+30}_{-30.6}$). The overlapping values, from different methods, found by Nandra et al. (1997), 9^{+18}_{-9} , and Hicks & Malkan (2008), $19.8 \pm 2.9^{\circ}$, exclude the fourth one derived by Fischer et al. (2013), 45.0° . Finally, the estimation made by Nandra et al. (1997) is preferred as it fully covers the potential inclination calculated by Hicks & Malkan (2008).

NGC 5548. Similar to the case of Mrk 509, the inclination of NGC 5548 evaluated by Nandra et al. (1997), $i = 10^{+80}_{-10}$, is rejected in favour of the one derived by Wu & Han (2001), $i = 47.3^{+7.6}_{-6.9}$.

NGC 7469. The viewing angle derived by Zhang & Wu (2002) is consistent with the one derived by Hicks & Malkan (2008), within the error bars of the later. The inclination of NGC 7469 estimated by Nandra et al. (1997) is not worth considering due to its huge error bars (20^{+70}_{-20}).

NGC 1068. Finally, the estimations of Fischer et al. (2013) and Hönig et al. (2007) are different and do not overlap. However, the inclination derived by Hönig et al. (2007) is supported by the three-dimensional structure of the nuclear region of NGC 1068 reconstructed by Kishimoto (1999) using a different set of observations. As Kishimoto (1999) de-

rived a similar, $\sim 70^{\circ}$, inclination, the estimation of Hönig et al. (2007) is thus favoured.

2.3 Revisited polarization of Seyfert 2s

Similarly to the inclination estimates in the previous section, I have found for a very few number of objects several continuum polarization measurements achieved by different authors. The level of polarization and the polarization position angle (measured from north through east) were coherent between the different observing campaigns, regardless of the epoch. I have thus favoured polarimetric measurement from Seyfert atlases (Martin et al. 1983; Brindle et al. 1990; Kay 1994; Ogle et al. 1999; Smith et al. 2002a).

However, not all of these measurements are reliable. Most, if not all, type-2 AGN are dominated by relatively large, unpolarized starlight fluxes (Antonucci 2002b). Removing the contribution from old stellar populations drastically increases the resulting continuum polarization but previous polarimetric type-2 atlases still recorded low, 1 – 3 %, polarization degrees (Martin et al. 1983; Kay 1994; Smith et al. 2002b). Such behaviour is in disagreement with the unified model, where radiation escapes from the inner parts of the obscuring equatorial torus by perpendicular scattering into the polar outflows, carrying a large amount of polarization (Antonucci 1993). High polarization percentages are thus expected, but not observed, for type-2 objects (Miller & Goodrich 1990). Miller & Goodrich (1990) reported that even after starlight subtraction, the remaining continuum is dominated by another component responsible for dilution of the polarized flux, now identified as originating from starburst regions. To estimate the continuum polarization of a given object after corrections for the interstellar polarization and dilution by host galaxy starlight, Tran (1995a,b,c) proposed to measure the equivalent width (EW) of the broad Balmer lines in both intensity and polarized flux spectra,

since polarized flux spectra have the advantage to suppress low polarization emission from starlight and narrow emission lines. If no additional unpolarized, or very little polarized, continuum superimposes on the polarization originating from the scattered light alone, the intrinsic polarization in the line and the adjacent continuum should be equal. This is the case for NGC 1068, where the broad lines have the same polarization as the continuum (Antonucci et al. 1994). Unfortunately, nearly all the remaining measurements of type-2 AGN polarization are likely to be biased downward.

In the following I revisit and, when necessary and possible, revise the estimated continuum polarization of type-2 objects to be included in the compendium. The best way to estimate the continuum polarization due only to scattered light is to divide the polarized flux by the total flux across the broad emission lines, as suggested by Tran (1995c) and Antonucci (2002a). Only the broad lines polarization is a reliable indicator of the polarization of the scattered component. However, by definition, broad lines are not detected in the total flux spectra of type-2s. To overcome this problem, I compare the typical EW of type-1 polarized, broad, Balmer emission lines H α λ 6563 (EW \approx 400 Å; Smith et al. 2002a) and H β λ 4861 (EW \approx 80 Å; Young et al. 1997) to the EW of the polarized H α λ 6563 and H β λ 4861 lines of the compendium-selected Seyfert 2s. This is a first-order approximation, but it is justified by the fact that the broad lines have the same EW in polarized flux in type-1 and type-2 AGN (Antonucci 2002b). If the ratio is equal to unity, the continuum polarization is correct; if larger than unity, the continuum must be revised by the same factor. In the case where no spectra are available to estimate the EW of broad emission lines in polarized flux, the continuum polarization reported by previous Seyfert atlases will be used as a lower limit (Goodrich & Miller 1994).

I revisit the polarization of the Circinus galaxy measured by Alexander et al. (2000), 1.9 %, using the only broad emission line detected in its polarized flux spectrum, namely H α λ 6563 (H β λ 4861 being only marginally detected, $\sim 2\sigma$). The EW, estimated using a Lorentzian profile (Kollatschny & Zetzl 2012), is about 34 Å. From then, the ratio between type-1 H α EW (\approx 400 Å) and EW_{H α Circinus} is equal to 11.8 and the resulting continuum polarization is equal to 22.4 %. Interestingly, Oliva et al. (1998) have derived a similar result (25 %) using a simple, numerical model applied to their own spectropolarimetric measurement of the Circinus galaxy.

Mrk 3 has been observed by Tran (1995a), who found after correction for interstellar polarization and dilution by starlight a continuum polarization of 7.0 %. Using H α λ 6563 and H β λ 4861 as diagnostic lines from Tran (1995b), the EW of H α is estimated to be \sim 360 Å and EW H β \sim 65 Å. The ratio are 1.11 and 1.23, respectively. The scattered light is thus expected to have an intrinsic polarization of 7.77 – 8.61 %.

The small bump around 6563 Å in the percentage of polarization spectrum of NGC 1667 was attributed to the red wing of the H α + [N II] profile by Barth, Filippenko & Moran (1999), who consequently stated that no polarized H α emission have been detected. However, the polarization spectra are dominated by high noise levels, probably hiding the appearance of the broad wings of the line. The EW of the

polarized H α λ 6563 line is consequently very similar to the EW measured in the total flux spectrum, i.e. 14.3 Å. The resulting ratio, 28.0, can be used to account for an upper limit of the intrinsic continuum polarization, which is then set between 0.35 % (Barth, Filippenko & Moran 1999) and 9.8 %.

Both H α λ 6563 and H β λ 4861 polarized broad lines can be detected in the polarized flux spectrum of NGC 4507 (Moran et al. 2000). The estimated EW are 165 Å (H α) and 30 Å (H β), raising the continuum polarization from its initial value (6.1 %; Moran et al. 2000) to 14.8 – 16.3 %.

NGC 5506 has been observed by Kay (1994), who found a continuum polarization of 2.60 % \pm 0.41 %. From the spectropolarimetric measurements of a sample of nearby Compton-thin ($N_{\text{H}} < 10^{23}$ cm $^{-2}$) Seyfert 2s, Lumsden et al. (2004) found no evidence for a broad H α λ 6563 line in NGC 5506. They argued that the cause of non-detection of the broad lines in the polarized spectrum of this AGN can be due to an extended obscuring region rather than non-existence. I estimate an upper limit on the EW for the polarized H α λ 6563 line (\sim 10 Å) looking at the total flux spectrum and set the corrected polarization degree between 2.6 % and 100 %.

Tran (1995b) measured the continuum polarization of NGC 7674 to be 3.8 % after removing the starlight contribution. From their spectra, I estimate the EW of the H α λ 6563 and H β λ 4861 lines to be 208 Å and 40 Å, respectively. The ratio are 1.72 and 2.0, increasing the intrinsic polarization of the scattered light to 6.54 – 7.6 %.

NGC 1068 has proven to be remarkable in a sense that the polarization degree of its broad emission lines is similar to that of the continuum. This peculiar feature is also shared by the broad H α line/continuum polarization in IRAS 13349+2438 and no revisions are necessary for these two objects. The high level of polarization detected in Mrk 78 by Kay (1994), 21.0 % \pm 9.0 %, is significantly different from the rest of the sample and might face the same physical conditions, if not suffering from an upward bias (since polarization is a positive-definite quantity). The absence of spectra make it impossible to verify this assumption.

The polarization spectra of the seven BAL quasars extracted from Ogle et al. (1999), 0019+0107, 0145+0416, 0226–1024, 0842+3431, 1235+1453, 1333+2840 and 1413+1143, are too noisy to measure the EW of isolated broad emission lines in polarized flux. The few broad emission lines detected in total flux are either merged with some other lines (L α + N V; Al III + C III), truncated or poorly resolved. Most of them are not even detected in polarized flux. The reported polarization continuum will then be used as lower limits.

Unfortunately, there are no detailed polarization spectra published so far for Mrk 34, Mrk 573, Mrk 1066 and NGC 5643.

Over the 20 type-2 AGN, 3 of them did not need any correction, 6 were revised and 11 can only be used as basic lower limits for the intrinsic polarization of the scattered light. Type-1 AGN, once corrected for starlight contribution, do not suffer from an additional dilution component and are thus directly exploitable. The detailed lists of the AGN sampled, with inclination matched to continuum po-

Object	Waveband (Å)	Pol. degree (%)	Pol. angle (°)	Ref.	Inclination (°)	Ref.	Method
3C 120	3800 – 5600	0.92 ± 0.25	103.5 ± 7.9	Mar83	22.0 ^{+9.3} _{-7.7}	Wu01	A
Akn 120	3800 – 5600	0.65 ± 0.13	78.6 ± 5.7	Mar83	42.0	Zha02	A
Akn 564	6000 – 7500	0.52 ± 0.02	87.0 ± 1.3	Smi02	26.0	Zha02	A
ESO 323-G077	3600	7.5	84	Sch03	45.0	Sch03	B
Fairall 9	3800 – 5600	0.4 ± 0.11	2.4 ± 7.6	Mar83	35.0	Zha02	A
Fairall 51	4700 – 7200	4.12 ± 0.03	141.2 ± 0.2	Smi02	45.0	Sch01	B
IC 4329A	5000 – 5800	5.80 ± 0.26	42.0 ± 1.0	Bri90	10 ^{+13.0} _{-10.0}	Nan97	C
PG 1211+143	4700 – 7200	0.27 ± 0.04	137.7 ± 4.5	Smi02	31.0	Zha02	A
MCG-6-30-15	5000 – 5800	4.06 ± 0.45	120.0 ± 3.0	Bri90	34.0 ^{+5.0} _{-6.0}	Nan97	C
Mrk 79	3800 – 5600	0.34 ± 0.19	0.4 ± 16.2	Mar83	58.0	Zha02	A
Mrk 110	3200 – 8600	0.17 ± 0.08	18.0 ± 15.0	Ber90	37.4 ^{+9.2} _{-9.5}	Wu01	A
Mrk 279	6000 – 7500	0.48 ± 0.04	58.9 ± 2.4	Smi02	35.0	Fis13	F
Mrk 335	3800 – 5600	0.48 ± 0.11	107.6 ± 6.9	Mar83	20.0	Zha02	A
Mrk 478	3800 – 5600	0.46 ± 0.15	44.9 ± 9.5	Mar83	25.0	Zha02	A
Mrk 486	3800 – 5600	3.40 ± 0.14	136.8 ± 1.2	Mar83	16.0	Zha02	A
Mrk 509	3800 – 5600	1.09 ± 0.15	146.5 ± 4.0	Mar83	19.0	Zha02	A
Mrk 590	3800 – 5600	0.32 ± 0.30	105.9 ± 26.6	Mar83	17.8 ^{+6.1} _{-5.9}	Wu01	A
Mrk 705	4700 – 7200	0.46 ± 0.07	49.3 ± 6.5	Smi02	16.0	Zha02	A
Mrk 707	3800 – 5600	0.20 ± 0.24	140.9 ± 52.0	Mar83	15.0	Zha02	A
Mrk 766	4500 – 7100	3.10 ± 0.80	90.0	Bat11	36.0 ^{+8.0} _{-7.0}	Nan97	C
Mrk 841	4500 – 7500	1.00 ± 0.03	103.4 ± 1.0	Smi02	26.0 ^{+8.0} _{-5.0}	Nan97	C
Mrk 896	3800 – 5600	0.55 ± 0.13	1.9 ± 7.1	Mar83	15.0	Zha02	A
Mrk 1239	3800 – 5600	4.09 ± 0.14	136.0 ± 1.0	Mar83	7.0	Zha02	A
NGC 1097	5100 – 6100	0.26 ± 0.02	178 ± 2.0	Bar99	34.0	Sto97	D
NGC 1365	5000 – 5900	0.91 ± 0.18	157 ± 6.0	Bri90	57.5 ± 2.5	Risa13	C
NGC 3227	5000	1.3 ± 0.1	133 ± 3.0	Sch85	14.2 ± 2.5	Hic08	E
NGC 3516	4500 – 7500	0.15 ± 0.04	30.1 ± 8.0	Smi02	26 ⁺³ ₋₄	Nan97	C
NGC 3783	4500 – 7500	0.52 ± 0.02	135.5 ± 1.0	Smi02	15.0	Fis13	F
NGC 4051	4500 – 7500	0.55 ± 0.04	82.8 ± 1.8	Smi02	19.6 ^{+10.4} _{-6.6}	Wu01	A
NGC 4151	4600 – 7400	0.26 ± 0.08	62.8 ± 8.4	Mar83	9 ⁺¹⁸ ₋₉	Nan97	C
NGC 4593	6000 – 7600	0.14 ± 0.05	109.5 ± 10.8	Smi02	21.6 ± 10.5	Wu01	A
NGC 5548	6000 – 7500	0.69 ± 0.01	33.2 ± 0.5	Smi02	47.3 ^{+7.6} _{-6.9}	Wu01	A
NGC 7469	6000 – 7500	0.18 ± 0.01	76.8 ± 1.7	Smi02	15.0 ± 1.8	Hic08	E

Table 2. Recorded average continuum polarization states and inclinations of 33 type-1 AGN. The first reference column is related to polarization measurements, the second to estimations of the orientation. Methods used to determine the inclination of the system are described in Sect. 2.1. Legend: Mar83 - Martin et al. (1983); Sch85 - Schmidt & Miller (1985); Ber90 - Berriman et al. (1990); Bri90 - Brindle et al. (1990); Nan97 - Nandra et al. (1997); Sto97 - Storchi-Bergmann et al. (1997); Bar99 - Barth, Filippenko & Moran (1999); Sch01 - Schmid et al. (2001); Wu01 - Wu & Han (2001); Smi02 - Smith et al. (2002a); Zha02 - Zhang & Wu (2002); Sch03 - Schmid, Appenzeller & Burch (2003); Hic08 - Hicks & Malkan (2008); Bat11 - Batcheldor et al. (2011); Fis13 - Fischer et al. (2013) and Ris13 - Risaliti et al. (2013).

larization, are given in Tab. 2 and Tab. 3, for type-1 and type-2 objects respectively.

2.4 Inclination versus polarization

The resulting compendium, comparing the polarization percentage P versus the inclination i for 53 objects, is presented in Fig. 1. Type-1 AGN are shown in red, type-2 AGN in violet.

According to the inclination estimations, type-1 AGN cover a range of orientation from $i = 0^\circ$ (pole-on) to $i = 45^\circ - 60^\circ$, which is in agreement with the estimations of the overall half opening angle of the system, $\theta > 58^\circ$, made by Osterbrock & Martel (1993) and Ho, Filippenko & Sargent (1995). Type-1 objects exhibit low polarization degrees ($\leq 1\%$), except for seven unusually, highly polarized sources (ESO 323-G077, Fairall 51, IC 4329A, MCG-6-30-15, Mrk 486, Mrk 766 and mrk 1239). Those high levels of polarization are similar to the detection of polarization degrees up to 4% in Mrk 231

(Gallagher et al. 2005), or in the Warm Infrared Ultraluminous AGN survey done by Hines (1994), but they still need to be explained (see Sect. 4.2). However, most of the type-1 sources collected here follow the empirical ascertainment, started with the observational surveys of Seyfert 1 AGN realized by Berriman (1989), Berriman et al. (1990) and Smith et al. (2002a): type-1 AGN predominantly show low levels of polarization, associated with polarization position angles roughly parallel² to the radio axis of the system (when radio axis measurements were available). It is particularly interesting to note that, among the seven polar scattering dominated AGN (with “perpendicular” polarization) identified, five exhibit a polarization degree higher than 1%. If a per-

² Exceptions in the compendium are NGC 5548, Fairall 51, Mrk 486 (Smith et al. 2002a), ESO 323-G077, NGC 3227, and probably Mrk 766 and NGC 4593 (Batcheldor et al. 2011), which exhibit polarization position angles perpendicular to their radio axis.

Object	Waveband (Å)	Pol. degree (%)	Pol. angle (°)	Ref.	Inclination (°)	Ref.	Method
0019+0107	4000 – 8600	> 0.98	35.0 ± 0.5	Ogl99	90.0	Bor10	H
0145+0416	1960 – 2260	> 2.14	126.0 ± 1.0	Ogl99	80.0	Bor10	H
0226-1024	4000 – 8600	> 1.81	167.1 ± 0.2	Ogl99	87.0	Bor10	H
0842+3431	4000 – 8600	> 0.51	27.1 ± 0.6	Ogl99	78.0	Bor10	H
1235+1453	1600 – 1840	> 0.75	175.0 ± 12.0	Ogl99	76.0	Bor10	H
1333+2840	4000 – 8600	> 4.67	161.5 ± 0.1	Ogl99	80.0	Bor10	H
1413+1143	4000 – 8600	> 1.52	55.7 ± 0.9	Ogl99	88.0	Bor10	H
Circinus	5650 – 6800	22.4 – 25.0	45.0	Ale00	65.0	Fis13	F
IRAS 13349+2438	3200 – 8320	23 – 35	124.0 ± 5.0	Wil92	52.0	Wil92	I
Mrk 3	5000	7.77 – 8.61	167.0	Tra95	85.0	Fis13	F
Mrk 34	3200 – 6200	> 3.92	53.0 ± 4.5	Kay94	65.0	Fis13	F
Mrk 78	3200 – 6200	21.0 ± 9.0	75.3 ± 11.2	Kay94	60.0	Fis13	F
Mrk 573	3200 – 6200	> 5.56	48.0 ± 2.0	Kay94	60.0	Fis13	F
Mrk 1066	3200 – 6200	> 1.99	135.1 ± 2.6	Kay94	80.0	Fis13	F
NGC 1068	3500 – 5200	16.0 ± 2.0	95.0	Mill83	70.0	Hon07	G
NGC 1667	5100 – 6100	0.35 – 9.8	94.0 ± 1.0	Bar99	72.0	Fis13	F
NGC 4507	5400 – 5600	14.8 – 16.3	37.0 ± 2.0	Mor00	47.0	Fis13	F
NGC 5506	3200 – 6200	> 2.6	72.8 ± 4.5	Kay94	80.0	Fis13	F
NGC 5643	5000 – 5900	> 0.75	57.0 ± 9.0	Bri90	65.0	Fis13	F
NGC 7674	3200 – 6200	6.54 – 7.6	31.0	Tra95	60.0	Fis13	F

Table 3. Recorded average continuum polarization states and inclinations of 20 type-2 AGN. The first reference column is related to polarization measurements, the second to estimations of the orientation. Methods used to determine the inclination of the system are described in Sect. 2.1. Legend: Mill83 - Miller & Antonucci (1983); Bri90 - Brindle et al. (1990); Wil92 - Wills et al. (1992); Kay94 - Kay (1994); Tra95 - Tran (1995a); Bar99 - Barth, Filippenko & Moran (1999); Ogl99 - Ogle et al. (1999); Ale00 - Alexander et al. (2000); Mor00 - Moran et al. (2000); Hon07 - Hönig et al. (2007); Bor10 - Borguet & Hutsemékers (2010) and Fis13 - Fischer et al. (2013).

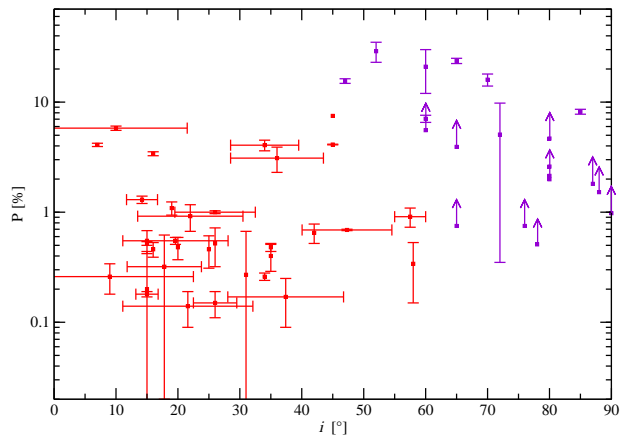


Figure 1. The polarization degree P is plotted versus the AGN inclination i . Type-1 Seyfert-like galaxies are shown in red, type-2 objects in violet.

pendicular polarization position angle can be explained by an increase of the opacity of the polar outflows (through which the observer’s line of sight is passing), it is more difficult to explain such high P at inclinations below 45° (Marin et al. 2012a).

In the case of type-2 AGN, objects show perpendicular polarization position angles associated with higher polarization percentages, not uncommonly $> 7\%$ (after first-order correction for the intrinsic continuum polarization). As electron-induced P depends on the cosine square of the

scattering angle, Seyfert galaxies seen edge-on are expected to be intrinsically more polarized (Miller & Antonucci 1983; Brindle et al. 1990; Kay 1994). Radiation scatters perpendicularly on to the ionized, polar outflows detected in type-2 AGN, leading to higher polarization percentages than at polar inclinations, where the combination of forward scattering and dilution by the unobscured nucleus diminishes the net polarization. A clear estimation of the average polarization percentage of Seyfert 2 objects remains problematic since most of the quoted values are lower limits. However, the trend is that P seems to increase with inclination, with a possible decrease at extreme type-2 inclinations that has to be properly observed by future, rigorous measurements of the scattered light alone. The overall inclination of Seyfert 2 AGN lies between 60° and 90° (edge-on).

No clear polarization break is detected at the transition angles ($45^\circ - 60^\circ$) between type-1 and type-2 objects; P increases continuously from pole-on to edge-on view. Note that the range of orientation that separates type-1 and type-2 Seyfert galaxies is not artificially enhanced by the selection criteria (see Sect. 2.2), as none of the rejected inclinations cover the $45^\circ - 60^\circ$ range. However, the reader is advised to note that possible bias in the estimation of i may shift some objects to different inclination values. ESO 323-G077 (type-1), NGC 1365 (type-1), IRAS 13349+2438 (type-2) and the Circinus galaxy (ESO 97-G13, type-2) are in the intermediate zone between the two classifications. While the type-2 classification of the Circinus galaxy is undisputed, the cases of ESO 323-G077, NGC 1365 and IRAS 13349+2438 are more ambiguous. Spectropolarimetric observations achieved by Schmid, Appenzeller & Burch (2003) showed that, at least, a fraction of the inner region of ESO 323-G077 must be hidden behind the torus horizon, classifying this AGN as a borderline

Seyfert 1 galaxy. NGC 1365 is another intriguing, borderline object, showing rapid transition between Compton-thin and Compton-thick regimes due to X-ray eclipses (Risaliti et al. 2005). Such behaviour leads to a difficult classification of NGC 1365, either type-1 (Schulz, Knake & Schmidt-Kaler 1994), type-1.5 (Veron et al. 1980), type-1.8 (Alloin et al. 1981; Risaliti et al. 2005) or even type-2 (Chun 1982; Rush et al. 1993). The case of IRAS 13349+2438 is somewhat similar to the previous object. The $H\beta$ line width measured by Lee et al. (2013) favours a type-2 classification, an argument in contradiction with Brandt et al. (1996) who found that IRAS 13349+2438 shares many properties with narrow-line Seyfert 1s, though they noted that this object must have a peculiar geometry. Such statement is supported by the spectropolarimetric observations realized by Wills et al. (1992), who have shown that the observer’s line of sight is probably intercepting part of the equatorial dusty material, classifying IRAS 13349+2438 as a borderline type-2 AGN. Thus, from a polarimetric point of view and if its estimated inclination is correct, the Circinus galaxy should be considered as a borderline Seyfert 2 object.

3 POLARIZATION PREDICTIONS FROM THEORETICAL MODELS

A direct application of this polarization/inclination study concerns radiative transfer in numerical AGN models. While more recent simulations tend to complexify in terms of morphology, composition and kinematic, testing the relevance of a model against observations is a significant consistency check. In the following section, I run Monte Carlo simulations on four different AGN models from the literature and compare the polarimetric results to the compendium.

Simulations of emission, multiple scattering and radiative coupling in complex AGN environments were achieved using STOKES (Goosmann & Gaskell 2007; Marin et al. 2012a), a public³ Monte Carlo code including scattering-induced polarization. The results presented hereafter are representative of each different model, characterized by a unique set of parameters. The resulting wavelength-independent polarization percentage is integrated over 2000 to 8000 Å. For consistency, the same input spectrum is used for all the models, namely an isotropic source emitting an unpolarized spectrum with a power-law SED $F_* \propto \nu^{-\alpha}$ ($\alpha = 1$). Finally, an important condition on the models investigated below is that, at least, they reproduce the expected polarization dichotomy (i.e. parallel polarization position angles for type-1 inclinations and perpendicular polarization position angles for type-2s).

3.1 Three-component AGN

According to the axisymmetric unified model (Antonucci 1993), the central supermassive black hole and its accretion disc, that radiates most of its bolometric luminosity in the UV/optical bands, are obscured by an equatorial, dusty torus. A common hypothesis is that the funnel of the

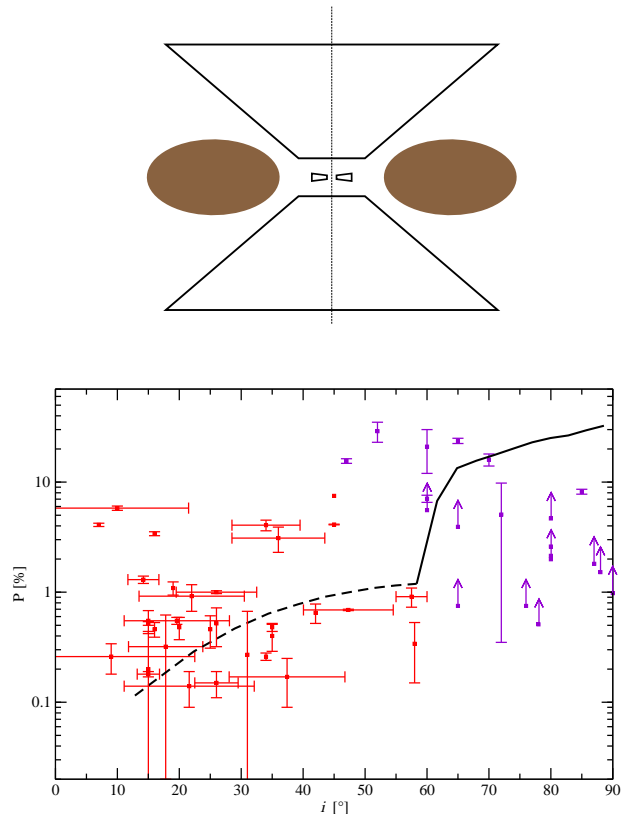


Figure 2. Top: schematic view of the three-component model. The dusty torus is shown in dark brown. Bottom: the resulting polarization (black line) of a three-component model (see Marin et al. 2012a) is plotted against observations. The dashed section corresponds to parallel polarization, the solid line to perpendicular polarization.

torus collimates ejection winds in the form of a bi-conical polar outflow. Past spectropolarimetric models of AGN, composed by a central irradiating source, a dusty torus and a bi-conical, electron-filled wind, showed that only perpendicular polarization (with respect to the symmetry axis of the torus) can emerge (Kartje 1995; Marin et al. 2012a). To introduce the production of parallel polarization in polar viewing angles, a third, equatorial region lying between the torus and the source has been proposed (Antonucci 1984; Young 2000). This highly ionized, geometrically thin disc can be associated with the accretion flow between the torus and the BLR (Young 2000; Goosmann & Gaskell 2007) and is necessary to reproduce the observed polarization dichotomy (Goosmann & Gaskell 2007; Marin et al. 2012a).

Following the parametrization from Marin et al. (2012a), the central, unpolarized source is surrounded by an equatorial, scattering flared disc with a half-opening angle of 20° with respect to the equatorial plane and a Thomson optical depth in the V band of $\tau_{disc} = 1$. Along the same plane, an optically thick ($\tau_{torus} \gg 1$), dusty torus, filled with a standard “Milky Way” dust mixture (Mathis, Rumpel & Nordsieck 1977) prevents radiation to escape along the equator. An hourglass-shaped, electron-filled region ($\tau_{wind} = 0.3$)

³ <http://www.stokes-program.info/>

accounts for the polar ejection flow. The torus and the collimated ionized wind sustain the same half-opening angle, 60° with respect to the symmetry axis of the model, see Fig. 2 (top). The reader may refer to Marin et al. (2012a) for further details about the model.

The wavelength-integrated polarization spectrum of the three-component model is shown in Fig. 2 (bottom). From 0° to 60° (where the transition between type-1 and type-2 classification occurs), the three-component model successfully reproduces the average polarization level expected from type-1 AGN (i.e. $P \leq 1\%$) as well as a parallel polarization position angle. P rises from pole-on view to intermediate inclination without exceeding 1%. When the observer's line of sight crosses the torus height, P decreases. This is due to the competition between parallel polarization produced by the equatorial, scattering disc and perpendicular polarization originating from the torus/polar regions, cancelling each other. Such behaviour is expected in any axisymmetric model and P may decrease down to zero, depending on the global morphology of the system. Once the equatorial, electron-filled disc disappears behind the torus horizon, P strongly increases, up to 30%, as radiation becomes dominated by perpendicular, Thomson scattering inside the polar outflows. The resulting polarization is not high enough in the $45^\circ - 65^\circ$ range and becomes too strong at large inclinations to fit the majority of type-2 objects.

3.2 Four-component AGN

A three-component NLR model produces too much polarization at extreme type-2 inclinations. A natural way to decrease the amount of P is to add an absorbing medium to the previous model. We know from observations that, beyond the dust sublimation radius, the ionized outflows merge continuously with the dusty environment of the host galaxy, forming the so-called (low-density) NLR (Capetti et al. 1996, 1999). The next step is then to investigate, in the framework of this compendium, the polarization signature of a four-component model that includes a dust-filled, low opacity ($\tau_{NLR} = 0.3$) NLR (Marin & Goosmann 2012). I used the same parametrization as in Sect. 3.1, with the NLR bi-cone sustaining the same half-opening angle as the ionized outflows (Fig. 3, top).

The addition of NLR into the modelling of an AGN does not strongly impact the overall polarization signature. It slightly decreases the net polarization in type-1 viewing angles (see Fig. 3, bottom) but does not alter its polarization position angle due to the large opening angle of the torus. However, the possibility to reach polarization degrees of few percents (such as for IC 4329A, MCG-6-30-15 or Mrk 766) becomes less likely due to absorption. The transition between parallel and perpendicular polarization occurs at the same inclination but the net polarization is lower, due to absorption. Finally, in comparison with observations, P is found to be still too small between $45^\circ < i < 65^\circ$ ($P \sim 1 - 10\%$).

3.3 Fragmented media

Optical and UV observations of the NLR of NGC 1068 (Evans et al. 1991; Capetti et al. 1995a; Capetti, Macchetto

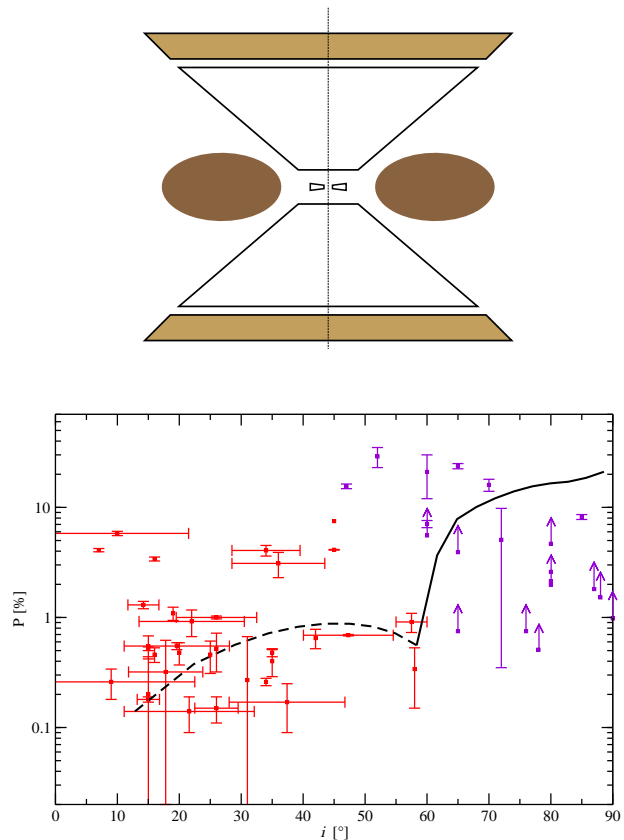


Figure 3. Top: schematic view of the four-component model. The model is the same as the three-component one with the addition of dusty NLR (shown in light brown). Bottom: the resulting polarization (black line) of a four-component model (see Marin & Goosmann 2012) is plotted against observations. The dashed section corresponds to parallel polarization, the solid line to perpendicular polarization.

& Lattanzi 1997; Packham et al. 1997) revealed the presence of many knots of different luminosity in the outflowing gas that can be attributed to inhomogeneities of the medium. Similar results are found for other sources (e.g. Mrk 3; Capetti et al. 1995b), strengthening the idea that AGN outflows may not be a continuous flow (Dai & Wang 2008). Due to the torus compactness, there is less direct evidence for a clumpy torus and most of the suppositions about the fragmented nature of the circumnuclear matter comes from numerical simulations (Pier & Krolik 1992, 1993; Nenkova, Ivezić & Elitzur 2002).

I now investigate a model in which the ionization cones are fragmented, while maintaining a compact dusty torus and an equatorial, scattering disc responsible for the production of parallel polarization. The equatorial disc and the circumnuclear dusty region retain the same morphological and composition parameters as in Sect. 3.1 and Sect. 3.2. The fragmented outflows now consist of 2000 electron-filled spheres of constant density ($\tau_{spheres} = 0.3$; Ogle et al. 2003) and radius (filling factor $\sim 5\%$). The filling factor is evaluated by summing up the volume of the clumps and dividing the total by the volume of the same unfragmented bi-conical

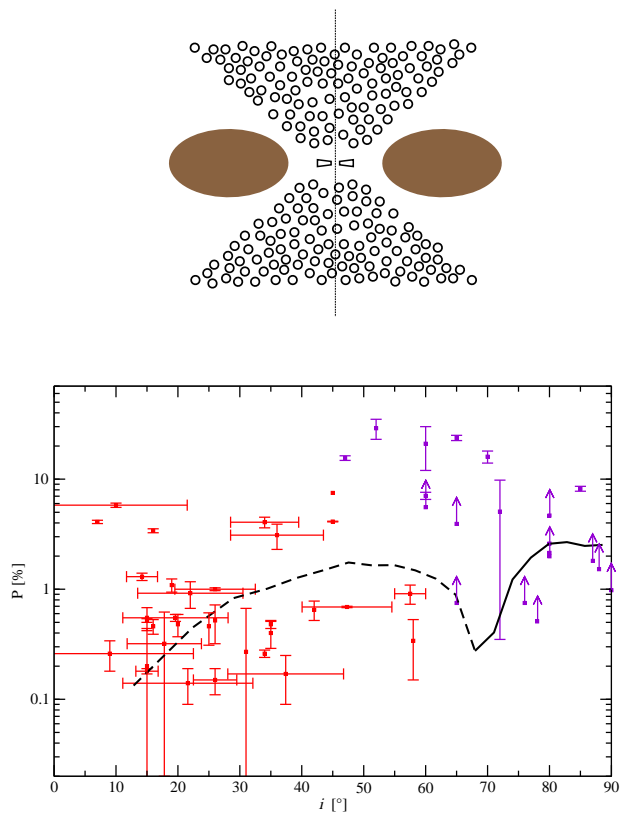


Figure 4. Top: schematic view of the clumpy model. The torus and the equatorial disc are the same as in Fig. 2. Bottom: the resulting polarization (black line) of a clumpy model is plotted against observations. The dashed section corresponds to parallel polarization, the solid line to perpendicular polarization.

NLR. A schematic view of the model is presented in Fig. 4 (top).

Similarly to the three and four-component models, a clumpy AGN (Fig. 4, bottom) reproduces both the low polarization levels and the expected polarization position angle in type-1 orientations. However, due to multiple scattering on the outflow’s clumps increasing the polarization degree, and gaps along the type-1 line of sights that allow a direct view of the electron disc, the net polarization percentage is higher, up to 2 % for intermediate inclinations. This level is still not sufficient to reproduce the observed polarization of highly polarized type-1 objects, but a fragmented medium enables higher polarization degrees for type-1 modelling. Fragmentation also impacts the inclination at which perpendicular polarization starts to dominate the production of parallel polarization, but the resulting transition inclination is not consistent with the observed polarization position angle of type-2 AGN. At type-2 inclinations, P is much lower ($P < 3$ %) than in previous modellings due to the enhanced escape probability from the outflows. A fragmented model can match the lower limit on polarization of a large fraction of type-2 AGN but fails to reproduce the high continuum polarization of NGC 1068, Mrk 78, IRAS 13349+2438 or the Circinus galaxy. However, the cloudlet distribution is probably different for each individual object and should be adapted case by case, i.e. by increasing/decreasing the

filling factor. By increasing the filling factor of the clumpy outflows, the model will start to behave like the AGN model presented in Sect. 3.1, strengthening the production of perpendicular polarization at type-2 viewing angles and matching higher polarization percentages.

3.4 A structure for quasars

The hydrostatic equilibrium hypothesis, postulated for the equatorial, toroidal region, is slowly evolving. Based on the pioneering work done by Blandford & McKee (1982), a hydrodynamical scenario is now considered as an alternative to the usual dusty torus, involving clumps of dusty matter embedded in a hydromagnetic disc-born wind (see Elitzur & Shlosman 2006, and references therein). Elvis (2000) took advantage of this scenario to build a model which attempts to explain the broad and narrow absorption line regions, as well as the broad emission line region, of type-1 quasars. In its phenomenologically derived structure, a flow of warm, highly ionized matter (WHIM) arises from an accretion disc in a narrow range of radii, bent outward and driven into a radial direction by radiation pressure. The model of Elvis (2000) was recently explored by Marin & Goosmann (2013a,b,c), who proposed a number of adjustments to match observed polarization data in the UV and optical bands.

To explore the consistency of the model described by Elvis (2000) and modified by Marin & Goosmann (2013a), I plotted in Fig. 5 (bottom) the adjusted model proposed by Marin & Goosmann (2013a). The WHIM bending angle is set to 45° and its collimation angle to 3° . It arises at a distance $r = 0.0032$ pc from the central source and extends up to 0.032 pc. The Thomson optical depth at the outflow’s base and inside the conical, outflowing direction are, respectively, set to $\tau_{base} = 0.02$ and $\tau_{flow} = 2$. A failed wind, composed of cold dust, is self-shielded from the continuum source by the WHIM. The dusty outflow sustains a half-opening angle of 51° with respect to the symmetry axis of the system, and a collimation angle of 3° . Its opacity along the equator is set to $\tau_{dust} = 4$. Refer to Marin & Goosmann (2013a) for details about this choice of parameters.

From Fig. 5 (bottom), it can be seen that the continuum polarization arising at type-1 inclinations follow the same trend as the three previous models: P reaches a maximum value of 1 % and cannot account for the highly polarized type-1 objects of the compendium. A local diminution of P appears at $i = 42^\circ$, when the observer’s line of sight crosses the outflowing material. The polarization position angle then switches from parallel to perpendicular, with respect to the projected symmetry axis of the system. While the transition between parallel and perpendicular polarization occurs at a smaller i in comparison with previous modelling, it is still coherent with the polarization position angle measurements of NGC 5548 and ESO 323-G077, which exhibit perpendicular polarization at $i = 47.3^{+7.6}_{-6.9}$ and $i = 45^\circ$, respectively. Beyond 54° , when the observer’s line of sight no longer passes through the radial outflows, P reaches 10 % – 11 % then slowly decreases because of the overwhelming impact of dust absorption along the equatorial direction. The polarization predicted by the line-driven wind model fits nearly all the observational, highly polarized type-2 objects in the $45^\circ - 65^\circ$ range and can account for objects

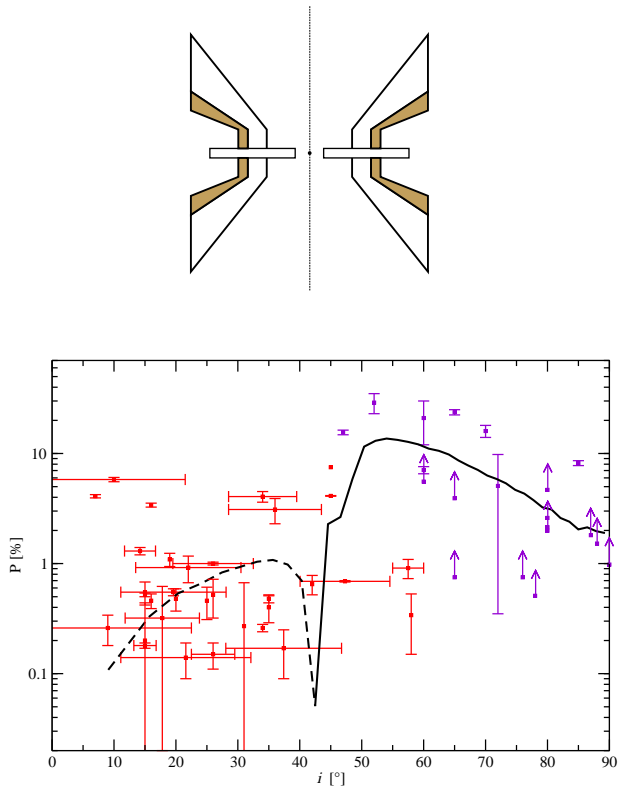


Figure 5. Top: schematic view of the structure for quasar as proposed by Elvis (2000) and modified by Marin & Goosmann (2013a). The WHIM appears in white, the failed dusty wind in brown. Bottom: the resulting polarization (black line) of the disc-born wind model is plotted against observations. The dashed section corresponds to parallel polarization, the solid line to perpendicular polarization.

with lower P at extreme inclinations. It is noteworthy that while a disc-born wind is by far the closest model to observations, one must be cautious as type-2 polarizations have first-order corrections and estimated inclinations are subject to potential biases.

4 DISCUSSION

4.1 AGN modelling within the compendium

The polarization-versus-inclination study presented in this paper allows a test of the relevance of four different AGN models from the literature. All of them successfully reproduce both the observed polarization dichotomy and the average polarization percentage of type-1 AGN, but strongly differ in the $45^\circ - 90^\circ$ inclination range. It is then easier to discriminate between several AGN models at intermediate inclinations. Models composed of uniform, homogeneous reprocessing regions (an equatorial scattering disc, a dusty torus and a pair of collimated cones, with the possible addition of dusty NLR) tend to create high perpendicular polarization degrees for type-2 AGN, while the polarization produced by a model with fragmented polar outflows do not extend farther than 3 % in the same orientation range.

Moreover, in the case of the model with clumpy ionization cones, the transition between parallel and perpendicular polarization happens at typical type-2 inclinations, which is in disagreement with observations. A refinement of the clumpy model is necessary. A deeper analysis of fragmented media is ongoing, targeting equatorial scattering discs, LIL and HIL BLR, tori, ionization cones and NLR. Preliminary results show that the polarization degree at type-2 inclinations can rise up to few tens of percent for dense cloudlet distributions. The transition between parallel and perpendicular polarization is correlated with the half-opening angle of the torus, and a fragmented circumnuclear region with a half-opening angle of 45° can produce a switch between parallel and perpendicular polarization position angle at $\sim 60^\circ$. The exploration of the parameter space of the models (optical depth, filling factor, covering factor ...) will be considered. The model of Elvis (2000) is undoubtedly the closest to observation, as it produces both high and low polarization degrees at type-2 viewing angle, strengthening the hypothesis that at least some undermined fraction of AGN components are wind-like structures.

4.2 Highly polarized type-1 AGN

Even by varying the parameters, none of the model can reach the high polarization levels of the inventoried type-1s ESO 323-G077 (7.5 %), Fairall 51 ($4.12\% \pm 0.03\%$), IC 4329A ($5.80\% \pm 0.26\%$), MCG-6-30-15 ($4.06\% \pm 0.45\%$), Mrk 486 ($3.40\% \pm 0.14\%$), Mrk 766 ($3.10\% \pm 0.80\%$), Mrk 1239 ($4.09\% \pm 0.14\%$) or Mrk 231 ($\sim 4\%$; Gallagher et al. 2005). Results presented in Sect. 2.4 show that their inclination ranges from 0° to 45° , indicating that scattering at large angles between the photon source, the polar winds and the observer is unlikely to be responsible for all the atypically high continuum polarization observed. As the optical thickness of AGN polar outflows is estimated to be relatively small ($\tau \ll 1$), the major contribution to scattering-induced type-1 polarization comes from the equatorial scattering disc. Goosmann & Gaskell (2007) showed that the resulting polarization percentage from an equatorial, electron-filled disc is fairly low, independently of its half opening angle and Thomson opacity. A major challenge to numerical models of AGN is to increase the net polarization degree at type-1 viewing angles for isolated cases. It is even more challenging taking into account that the polarization position angle of five out of the seven objects (ESO 323-G077, Fairall 51, Mrk 486, Mrk 766 and NGC 3227) is found to be perpendicular to their radio axis, similarly to Mrk 231 (Smith et al. 2004).

There are several potential ways to strengthen the net polarization of the models. One can consider perpendicular scattering between the source, a reprocessing region located along the equatorial plane, and the observer. A promising target could be the HIL and LIL BLR. Considering the constraints on the HIL and LIL BLR structure derived by Kollatschny & Zetzl (2013), using kinematic measurements of emission lines in four nearby AGN, one can estimate the half-opening angle of the emission line region. According to Kollatschny & Zetzl (2013), the HILs (i.e. emitted close to the photoionizing source) originate from a medium with half-opening angle $3.8^\circ - 26^\circ$ from the equatorial plane, while the LILs are created in a structure with a half-opening

angle $11^\circ - 60^\circ$. Further tests must be achieved to explore the polarization position angle and the amount of parallel polarization that HIL and LIL BLR can generate but it is unlikely that scattering within an axisymmetrical model can reach up to few percents at type-1 inclinations.

As stated by Gaskell (2010, 2011), breaking the symmetric pattern of irradiation can help to understand the velocity dependence of broad emission line variability detected in many AGN. Strong off-axis flares could then explain the observed, extremely asymmetric, Balmer lines with broad peak redshifted or blueshifted by thousands of $\text{km}\cdot\text{s}^{-1}$ (Smith et al. 2002a), and produce higher polarization degrees even at polar orientation. It is important to test the off-axis flare model as, if correct, the azimuthal phase of the continuum source would play a critical role in the measurement of the supermassive black hole mass. Goosmann, Gaskell & Marin (2013) have recently started the investigation of the off-axis irradiation theory by looking at the velocity dependence of the polarization of the broad emission lines. Preliminary results, compared to spectropolarimetric data for type-1 AGN from the literature, indicate that both the degree and position angle of polarization should be affected by asymmetrical emission. The net polarization percentage of the optical continuum is also slightly stronger. Further modelling will be achieved to explore how far optical and UV continuum polarization can be strengthened by temporary off-axis irradiation.

Finally, highly polarized AGN are not uncommon in type-1 radio-loud objects, with P up to $45.5\% \pm 0.9\%$ (Mead et al. 1990). The net polarization is quite variable from the radio to the optical band, often on short time-scales, pointing towards well-ordered magnetic fields surrounding a spatially small emitting region. While most of the observed polarization of radio-quiet AGN is undoubtedly originating from scattering off small particles (Stockman et al. 1979; Antonucci 1984, 1993), the high, optical polarization of blazing quasars is thought to be associated with Doppler-boosted synchrotron emission from relativistic jets pointing towards us. The polarization position angle of blazar cores is usually perpendicular to the jet axis while a parallel component is detected for emerging superluminal knots (D’arcangelo et al. 2009). If electron and dust reprocessing appear to be unable to reach $P \geq 3\%$ along poloidal directions, the correct interpretation might lie somewhere in the middle. The presence of a sub-parsec, aborted jet has yet to be proven but could explain the time variability and spectra of Narrow Line Seyfert 1 galaxies (Ghisellini et al. 2004) and potentially create perpendicular polarization degree up to a few percent, while the lines and continuum polarization would be still mainly produced by reprocessing. If an undetermined fraction of the total polarization of highly polarized type-1 AGN indeed originates from synchrotron emission, the net polarization could be expected to vary, but with a much smaller amplitude than for synchrotron-dominated, radio-loud objects. Long term monitoring of radio-quiet, highly-polarized type-1 AGN would then help to evaluate the fraction of polarization arising from reprocessing and from synchrotron emission.

4.3 Potential caveats on the determination of inclination

Estimations made by Wu & Han (2001) and Zhang & Wu (2002) are primarily based on the assumptions that Seyfert 1 and normal galaxies follow the same black hole mass⁴ - bulge velocity dispersion correlation, and that the LIL BLR are in pure Keplerian rotation, coplanar to the system inclination. While detected, the motion and the morphology of the LIL BLR remain uncertain (Peterson 2006). There are no strong constraints from the emission line profiles as a wide variety of kinematic models are able to reproduce the non-Gaussian profiles detected in AGN (Bon et al. 2009). The technique of velocity-resolved reverberation mapping (Gaskell 1988) is a step forward and tends to rule out any significant outflow from the AGN, while detecting a slight inflow (Gaskell et al. 2007) and fast Keplerian motion.

Fitting the distorted red wing of the Fe $K\alpha$ fluorescent line in X-ray bright, type-1 AGN can lead to possible bias. The procedure used by Nandra et al. (1997) assumes that the asymmetrical broadening of the iron line is caused by Doppler and general relativistic effects close to the central black hole; however, a competitive mechanism was proposed by Inoue & Matsumoto (2003); Miller, Turner & Reeves (2008, 2009) and Miller & Turner (2013). In this scenario, line broadening occurs at larger distances from the accretion disc, where a distribution of cold, absorbing gas blocks a fraction of the initial continuum. Transmitted and scattered radiation through the cloulet environment finally carves out the distorted red wing. If distant absorption dominates relativistic effects, the estimated inclinations might then be questionable⁵.

The method developed by Fischer et al. (2013), based on the work achieved by Crenshaw et al. (2000) and Das et al. (2005, 2006), relies on the nature of the NLR kinematics to determine the orientation of the system. One of their fundamental hypothesis is consistent with the unified model: AGN are axisymmetrical objects. In this picture, the NLR structure sustains the same symmetry axis as the dusty torus, which is coplanar with the accretion disc. Thus, determining the inclination of the NLR is equivalent to determining the orientation of the whole system. However, a recent IR interferometric campaign carried out by Raban et al. (2009) found that the extended outflows of NGC 1068 are likely to be inclined by 18° with respect to the obscuring torus axis. If this trend is confirmed, and observed for other Seyfert-like galaxies, the overall AGN picture will become more complex.

Finally, the two-component model produced by Borguet & Hutsemékers (2010) shows degeneracies between the various parameter combinations. It disallows the characterization of the outflow geometry in quasars showing broad absorption features, and weakens the constraints brought on the inclination of the system. The viewing angles of the outflow derived by the authors are quite large, a conclusion shared by Schmidt & Hines (1999) and Ogle et al. (1999),

⁴ To rectify black hole masses obtained from reverberation mapping, a correction factor $f = 5$ was used by Ho (1999).

⁵ In this context, a future X-ray polarimetric mission would be a solid tool to identify the preponderant mechanism responsible for line distortion (Marin et al. 2012b; Marin & Tamborra 2013; Marin et al. 2013).

based on optical polarization surveys of BAL quasars, but contested by several other authors (Barvainis & Lonsdale 1997; Punsly & Zhang 2010). In particular, Punsly & Zhang (2010) showed that two-thirds of the BAL quasars they observed using $H\beta$ line width as a diagnostic are well represented by objects with gas flowing along polar directions.

5 CONCLUSIONS

The first match of 53 AGN inclinations with their intrinsic continuum polarization originating from electron and dust scattering is presented in this paper. Different techniques to retrieve the nuclear orientation of type-1 and type-2 Seyfert galaxies were presented and discussed, highlighting their potential caveats. The continuum polarization of several Seyfert-2s was corrected using broad $H\alpha$ and $H\beta$ line polarization as a reliable indicator of the true polarization of the scattered light, and lower limits were put for the remaining AGN whose polarization spectra were either noise-saturated or unpublished.

The resulting compendium⁶ is in agreement with past observational/theoretical literature, and warrants additional conclusions and remarks the following.

- Seyfert 1 AGN are associated with low polarization degrees, $P \leq 1\%$, and predominantly characterized by a polarization position angle parallel to the projected radio axis of the system. The inclination of type-1 objects ranges from 0° to 60° .

- Seven type-1s have been identified as polar scattering dominated AGN, i.e. showing a perpendicular polarization position angle. Among them, five have an atypical continuum polarization higher than 1% , mostly associated with $10^\circ - 45^\circ$ inclinations. As scattering-induced polarization is unlikely to produce such high polarization degrees at type-1 orientation, a more elaborate scenario must be considered.

- After correction, Seyfert 2 AGN show polarization degrees higher than 7% and perpendicular polarization position angle. Unfortunately, most of the objects have only lower limits. The inclination of type-2 objects is ranging from 47° to 90° .

- The transition between type-1 and type-2 AGN occurs between $45^\circ - 60^\circ$. This range of inclination is likely to include AGN classified as borderline objects, where the observer's line of sight crosses the horizon of the equatorial dusty medium. Four objects lie in this range, three of them (ESO 323-G077, NGC 1365 and IRAS 13349+2438) being already considered as borderline Seyfert galaxies from spectroscopic observations. If the estimated inclination of the fourth object (the Circinus galaxy) is correct, it should be considered as another borderline AGN.

- The usual axisymmetric AGN models have difficulties to reproduce the trend of polarization with inclination. Fragmenting the reprocessing regions is helpful to cover a wide range of continuum polarization but a disc-born wind model is found to be already quite close from observations. A fine

tuning of the line-driven disc wind could easily match a substantial fraction of the reported measurements.

Problems determining the inclination of AGN must be taken into consideration but, despite potential caveats, the associated continuum polarization lies within the margins of past empirical results, consolidating the basis of the compendium. It is then important for future models, as a consistency check, to reproduce the average continuum polarization, the polarization dichotomy and the transition between type-1 and type-2 classification ($45^\circ < i < 60^\circ$). By improving the quality of the methods to determine the inclination of AGN and properly removing the contribution of both stellar and starburst light in future polarimetric measurement of type-2 objects, it will be possible to bring very strong constraints on the morphology, composition and kinematics of AGN. To achieve this goal, a new UV/optical spectropolarimetric atlas of Seyfert 2s is necessary.

ACKNOWLEDGEMENTS

The author is grateful to the referee Ski Antonucci for his useful and constructive comments on the manuscript. I also acknowledge the Academy of Sciences of the Czech Republic for its hospitality, and the French grant ANR-11-JS56-013-01 of the project POLIOPTIX and the COST Action MP1104 for financial support.

REFERENCES

- Alexander, D. M.; Heisler, C. A.; Young, S.; Lumsden, S. L.; Hough, J. H.; Bailey, J. A. 2000, MNRAS, 313, 815
- Alloin, D., Edmunds, M. G., Lindblad, P. O., & Pagel, B. E. J. 1981, A&A, 101, 377
- Antonucci, R. R. J. 1984, ApJ, 278, 499
- Antonucci, R. R. J., & Miller, J. S. 1985, ApJ, 297, 621
- Antonucci, R. 1993, ARA&A, 31, 473
- Antonucci, R., Hurt, T., & Miller, J. 1994, ApJ, 430, 210
- Antonucci, R. 2002a, AGN Surveys, Proceedings of IAU Colloquium 184, ASP Conference Proceedings, Vol. 284. Edited by R.F. Green, E.Ye. Khachikian, and D.B. Sanders. San Francisco, CA: Astronomical Society of the Pacific, 2002, p. 147.
- Antonucci, R. 2002b, Astrophysical spectropolarimetry. Proceedings of the XII Canary Islands Winter School of Astrophysics, 2000, edited by J. Trujillo-Bueno, F. Moreno-Insertis, and F. Sanchez. Cambridge, UK: Cambridge University Press, ISBN 0-521-80998-3, 2002, p. 151 - 175
- Bambi, C. 2011, Modern Physics Letters A, 26, 2453
- Bambi, C. 2013, The Astronomical Review, 8, 010000
- Barth, A. J., Filippenko, A. V., & Moran, E. C. 1999, ApJ, 525, 673
- Barvainis, R., & Lonsdale, C. 1997, AJ, 113, 144
- Batchelder, D.; Robinson, A.; Axon, D. J.; Young, S.; Quinn, S.; Smith, J. E.; Hough, J.; Alexander, D. M. 2011, ApJ, 738, 90
- Berriman, G. 1989, ApJ, 345, 713

⁶ The compendium will be regularly updated and available upon email request.

- Berriman, G., Schmidt, G. D., West, S. C., & Stockman, H. S. 1990, *ApJS*, 74, 869
- Blandford, R. D., & McKee, C. F. 1982, *ApJ*, 255, 419
- Bon, E., Gavrilović, N., La Mura, G., & Popović, L. Č. 2009, *NewAR*, 53, 121
- Borguet, B., & Hutsemékers, D. 2010, *A&A*, 515, A22
- Brandt, W. N., Fabian, A. C., & Pounds, K. A. 1996, *MNRAS*, 278, 326
- Brindle, C.; Hough, J. H.; Bailey, J. A.; Axon, D. J.; Ward, M. J.; Sparks, W. B.; McLean, I. S. 1990, *MNRAS*, 244, 577
- Capetti, A., Axon, D. J., Macchetto, F., Sparks, W. B., & Boksenberg, A. 1995, *ApJ*, 446, 155
- Capetti, A., Macchetto, F., Axon, D. J., Sparks, W. B., & Boksenberg, A. 1995, *ApJ*, 448, 600
- Capetti, A., Axon, D. J., Macchetto, F., Sparks, W. B., & Boksenberg, A. 1996, *ApJ*, 469, 554
- Capetti, A., Macchetto, F. D., & Lattanzi, M. G. 1997, *Ap&SS*, 248, 245
- Capetti, A., Axon, D. J., Macchetto, F. D., Marconi, A., & Winge, C. 1999, *MmSAI*, 70, 41
- Chun, M.-S. 1982, *Journal of Korean Astronomical Society*, 15, 41
- Crenshaw, D. M., Kraemer, S. B., Hutchings, J. B., et al. 2000, *AJ*, 120, 1731
- D'arcangelo, F. D., Marscher, A. P., Jorstad, S. G., et al. 2009, *ApJ*, 697, 985
- Dai, H.-F., & Wang, T.-G. 2008, *ChJAA*, 8, 245
- Das, V., Crenshaw, D. M., Hutchings, J. B., et al. 2005, *AJ*, 130, 945
- Das, V., Crenshaw, D. M., Kraemer, S. B., & Deo, R. P. 2006, *AJ*, 132, 620
- Efron, B. 1979, *Bootstrap methods: Another look at the jackknife*. *Ann. Statist.* 7, 1
- Elitzur, M., & Shlosman, I. 2006, *ApJL*, 648, L101
- Evans, I. N.; Ford, H. C.; Kinney, A. L.; Antonucci, R. R. J.; Armus, L.; Caganoff, S. 1991, *ApJL*, 369, L27
- Elvis, M. 2000, *ApJ*, 545, 63
- Eracleous, M., Livio, M., Halpern, J. P., & Storchi-Bergmann, T. 1995, *ApJ*, 438, 610
- Fabian, A. C., Rees, M. J., Stella, L., & White, N. E. 1989, *MNRAS*, 238, 729
- Ferrarese, L., & Merritt, D. 2000, *ApJL*, 539, L9
- Fischer, T. C., Crenshaw, D. M., Kraemer, S. B., & Schmitt, H. R. 2013, *arXiv:1308.4129*
- Gallagher, S. C.; Schmidt, Gary D.; Smith, Paul S.; Brandt, W. N.; Chartas, G.; Hylton, Shavonne; Hines, D. C.; Brotherton, M. S. 2005, *ApJ*, 633, 71
- Gaskell, C. M. 1988, *ApJ*, 325, 114
- Gaskell, C. M., Klimek, E. S., & Nazarova, L. S. 2007, *arXiv:0711.1025*
- Gaskell, C. M. 2010, *arXiv:1008.1057*
- Gaskell, C. M. 2011, *Baltic Astronomy*, 20, 392
- Gebhardt, K., Bender, R., Bower, G., et al. 2000, *ApJL*, 539, L13
- Ghisellini, G., Haardt, F., & Matt, G. 2004, *A&A*, 413, 535
- Goodrich, R. W., & Miller, J. S. 1994, *ApJ*, 434, 82
- Goosmann, R. W., & Gaskell, C. M. 2007, *A&A*, 465, 129
- Goosmann, R. W., & Matt, G. 2011, *MNRAS*, 415, 3119
- Goosmann, R. W., Gaskell, C. M., & Marin, F. 2013, *arXiv:1311.2249*
- Hicks, E. K. S., & Malkan, M. A. 2008, *ApJS*, 174, 31
- Hines, D. C. 1994, Ph.D. Thesis, Texas University
- Ho, L. C., Filippenko, A. V., & Sargent, W. L. 1995, *ApJS*, 98, 477
- Ho, L. 1999, *ASSL*, 234, 157
- Hönig, S. F., Beckert, T., Ohnaka, K., & Weigelt, G. 2007, *The Central Engine of Active Galactic Nuclei*, 373, 487
- Inoue, H., & Matsumoto, C. 2003, *PASJ*, 55, 625
- Jaffe, W., Meisenheimer, K., Röttgering, H. J. A., et al. 2004, *Nature*, 429, 47
- Keel, W. C. 1980, *AJ*, 85, 198
- Kartje, J. F. 1995, *ApJ*, 452, 565
- Kay, L. E. 1994, *ApJ*, 430, 196
- Kishimoto, M. 1999, *ApJ*, 518, 676
- Kollatschny, W., & Zetzl, M. 2012, *arXiv:1211.3065*
- Kollatschny, W., & Zetzl, M. 2013, *A&A*, 558, A26
- Lawrence, A., & Elvis, M. 1982, *ApJ*, 256, 410
- Lee, J. C., Kriss, G. A., Chakravorty, S., et al. 2013, *MNRAS*, 430, 2650
- Lumsden, S. L., Alexander, D. M., & Hough, J. H. 2004, *MNRAS*, 348, 1451
- Macchetto, F.; Marconi, A.; Axon, D. J.; Capetti, A.; Sparks, W.; Crane, P. 1997, *ApJ*, 489, 579
- Maiolino, R., & Rieke, G. H. 1995, *ApJ*, 454, 95
- Marin, F., Goosmann, R. W., Gaskell, C. M., Porquet, D., & Dovčiak, M. 2012a, *A&A*, 548, A121
- Marin, F., & Goosmann, R. W. 2012, *SF2A-2012: Proceedings of the Annual meeting of the French Society of Astronomy and Astrophysics*. Eds.: S. Boissier, P. de Laverny, N. Nardetto, R. Samadi, D. Valls-Gabaud and H. Wozniak, pp.587-590
- Marin, F., Goosmann, R., & Dovčiak, M. 2012, *Journal of Physics Conference Series*, 372, 012065
- Marin, F.; Goosmann, R. W.; Doviak, M.; Muleri, F.; Porquet, D.; Grosso, N.; Karas, V.; Matt, G. 2012b, *MNRAS*, 426, L101
- Marin, F., & Goosmann, R. W. 2013, *MNRAS*, 436, 2522
- Marin, F., & Goosmann, R. W. 2013b, *SF2A-2013: Proceedings of the Annual meeting of the French Society of Astronomy and Astrophysics*. Eds.: L. Cambresy, F. Martins, E. Nuss, A. Palacios, pp.475-478
- Marin, F., & Goosmann, R. W. 2013c, *SF2A-2013: Proceedings of the Annual meeting of the French Society of Astronomy and Astrophysics*. Eds.: L. Cambresy, F. Martins, E. Nuss, A. Palacios, pp.479-482
- Marin, F., & Tamborra, F. 2013, *ASR*, in press, *arXiv:1309.1684*
- Marin, F.; Porquet, D.; Goosmann, R. W.; Doviak, M.; Muleri, F.; Grosso, N.; Karas, V. 2013, *MNRAS*, 436, 1615
- Marscher, Alan P.; Jorstad, Svetlana G.; Gómez, José-Luis; Aller, Margo F.; Teräsranta, Harri; Lister, Matthew L.; Stirling, Alastair M. 2002, *Nature*, 417, 625
- Martin, P. G., Thompson, I. B., Maza, J., & Angel, J. R. P. 1983, *ApJ*, 266, 470
- Mathis, J. S., Rumpl, W., & Nordsieck, K. H. 1977, *ApJ*, 217, 425
- Mead, A. R. G.; Ballard, K. R.; Brand, P. W. J. L.; Hough, J. H.; Brindle, C.; Bailey, J. A. 1990, *A&AS*, 83, 183
- Merritt, D., & Ferrarese, L. 2001, *ApJ*, 547, 140
- Moran, E. C., Barth, A. J., Kay, L. E., & Filippenko, A. V. 2000, *ApJL*, 540, L73
- Miller, J. S., & Antonucci, R. R. J. 1983, *ApJL*, 271, L7
- Miller, J. S., & Goodrich, R. W. 1990, *ApJ*, 355, 456

- Miller, L., Turner, T. J., & Reeves, J. N. 2008, *A&A*, 483, 437
- Miller, L., Turner, T. J., & Reeves, J. N. 2009, *MNRAS*, 399, L69
- Miller, L., & Turner, T. J. 2013, *ApJL*, 773, L5
- Nandra, K., George, I. M., Mushotzky, R. F., Turner, T. J., & Yaqoob, T. 1997, *ApJ*, 477, 602
- Nenkova, M., Ivezić, Ž., & Elitzur, M. 2002, *ApJL*, 570, L9
- Ogle, P. M.; Cohen, M. H.; Miller, J. S.; Tran, H. D.; Goodrich, R. W.; Martel, A. R. 1999, *ApJS*, 125, 1
- Ogle, P. M., Brookings, T., Canizares, C. R., Lee, J. C., & Marshall, H. L. 2003, *A&A*, 402, 849
- Oliva, E., Marconi, A., Cimatti, A., & Alighieri, S. D. S. 1998, *A&A*, 329, L21
- Osterbrock, D. E. 1978, *Proceedings of the National Academy of Sciences of the United States of America*, Volume 75, Issue 2, pp. 540-544
- Osterbrock, D. E., & Martel, A. 1993, *ApJ*, 414, 552
- Packham, C., Young, S., Hough, J. H., Axon, D. J., & Bailey, J. A. 1997, *MNRAS*, 288, 375
- Peterson, B. M. 2006, *Physics of Active Galactic Nuclei at all Scales*, 693, 77
- Pier, E. A., & Krolik, J. H. 1992, *ApJ*, 401, 99
- Pier, E. A., & Krolik, J. H. 1993, *ApJ*, 418, 673
- Punsly, B., & Zhang, S. 2010, *ApJ*, 725, 1928
- Raban, D., Jaffe, W., Röttgering, H., Meisenheimer, K., & Tristram, K. R. W. 2009, *MNRAS*, 394, 1325
- Reeves, J. N., Fabian, A. C., Kataoka, J., et al. 2006, *Astronomische Nachrichten*, 327, 1
- Risaliti, G., Elvis, M., Fabbiano, G., Baldi, A., & Zezas, A. 2005, *ApJL*, 623, L93
- Risaliti, G., Harrison, F. A., Madsen, K. K., et al. 2013, *Nature*, 494, 449
- Rowan-Robinson, M. 1977, *ApJ*, 213, 635
- Rush, B., Malkan, M. A., & Spinoglio, L. 1993, *ApJS*, 89, 1
- Schmid, H. M.; Appenzeller, I.; Camenzind, M.; Dietrich, M.; Heidt, J.; Schild, H.; Wagner, S. 2001, *A&A*, 372, 59
- Schmid, H. M., Appenzeller, I., & Burch, U. 2003, *AAP*, 404, 505
- Schmidt, G. D., & Miller, J. S. 1985, *ApJ*, 290, 517
- Schmidt, G. D., & Hines, D. C. 1999, *ApJ*, 512, 125
- Schulz, H., Knake, A., & Schmidt-Kaler, T. 1994, *A&A*, 288, 425
- Smith, P. S., Schmidt, G. D., Hines, D. C., Cutri, R. M., & Nelson, B. O. 2002b, *ApJ*, 569, 23
- Smith, J. E.; Young, S.; Robinson, A.; Corbett, E. A.; Gianuzzo, M. E.; Axon, D. J.; Hough, J. H. 2002a, *MNRAS*, 335, 773
- Smith, J. E.; Robinson, A.; Alexander, D. M.; Young, S.; Axon, D. J.; Corbett, Elizabeth A. 2004, *MNRAS*, 350, 140
- Stockman, H. S., Angel, J. R. P., & Miley, G. K. 1979, *ApJL*, 227, L55
- Storchi-Bergmann, T., Baldwin, J. A., & Wilson, A. S. 1993, *ApJL*, 410, L11
- Storchi-Bergmann, Thaisa; Eracleous, Michael; Livio, Mario; Wilson, Andrew S.; Filippenko, Alexei V.; Halpern, Jules P. 1995, *ApJ*, 443, 617
- Storchi-Bergmann, Thaisa; Eracleous, Michael; Ruiz, Maria Teresa; Livio, Mario; Wilson, Andrew S.; Filippenko, Alexei V. 1997, *ApJ*, 489, 87
- Tran, H. D. 1995, *ApJ*, 440, 565
- Tran, H. D. 1995, *ApJ*, 440, 578
- Tran, H. D. 1995, *ApJ*, 440, 597
- Veron, P., Lindblad, P. O., Zuiderwijk, E. J., Veron, M. P., & Adam, G. 1980, *A&A*, 87, 245
- Wills, Beverley J.; Wills, D.; Evans, Neal J., II; Natta, A.; Thompson, K. L.; Breger, M.; Sitko, M. L. 1992, *ApJ*, 400, 96
- Wittkowski, M.; Kervella, P.; Arsenault, R.; Paresce, F.; Beckert, T.; Weigelt, G. 2004, *A&A*, 418, L39
- Wu, X.-B., & Han, J. L. 2001, *ApJL*, 561, L59
- Young, S., Hough, J. H., Axon, D. J., & Bailey, J. A. 1997, *IAU Colloq. 163: Accretion Phenomena and Related Outflows*, ed. D. T. Wickramasinghe; G. V. Bicknell; and L. Ferrario, 121, 837
- Young, S. 2000, *MNRAS*, 312, 567
- Zhang, T.-Z., & Wu, X.-B. 2002, *ChJAA*, 2, 487

This paper has been typeset from a $\text{\TeX}/\text{\LaTeX}$ file prepared by the author.